ELSEVIER

Journal of Nuclear Materials 266–269 (1999) 1091–1096

journal of nuclear materials

Dynamic behavior of hydrogen isotopes in tungsten–carbon composite materials

T. Horikawa, B. Tsuchiya, K. Morita *

Department of Crystalline Materials Science/ Department of Nuclear Engineering, Graduate School of Engineering, Nagoya University, Furo-cho, Chikusa-ku, Nagoya 464-8603, Japan

Abstract

The thermal re-emission of hydrogen isotopes from WC layers on graphite, implanted with 5 keV H_2^+ and D_2^+ ion beams up to saturation at room temperature, has been studied by means of the elastic recoil detection (ERD) technique. It is found on isochronal annealing for 10 min that the re-emission takes place in three stages: the first stage occurs for retained fraction of 1.0–0.6, the second stage for retained fractions of 0.6–0.2 and the third stage below the retained fraction of 0.2, which is ascribed to re-emission from carbon segregated in the grain boundaries of the WC layers. It is also found on isothermal annealing that the concentration of retained hydrogen decreases rapidly in the beginning and hereafter very gradually with increasing the annealing time. The isothermal re-emission curves have been analyzed by taking into account the two trapping sites and the mass balance equations with two kinds of thermal detrapping ($\Sigma_{d_1}, \Sigma_{d_2}$), retrapping ($\Sigma t$) and local molecular recombination (K_1) between free hydrogen atoms. The isotope difference of the rate constants for elementary processes determined by best fitting of the solution to the experimental re-emission profiles is discussed with relevance to the nature of two trapping sites.

Keywords: Carbon composition; Hydrogen; Ion beam analysis; Local molecular recombination; Re-emission; Tungsten; Thermal detrapping

1. Introduction

In future fusion devices, high Z refractory metal and carbon are planned to be used simultaneously as the divertor plate and the first wall armor, respectively. The mutual redeposition of sputtered substances modifies the surface layers of the materials into metal carbides under plasma irradiation at high temperatures for long term discharge.

Refractory metal carbides have the desired property of low sputtering yield [1]. There is a concern that the sputtering of high Z metal induces radiative cooling of the hot core plasma, but TiC and WC layers coated on graphite have shown that the sputtering of metals is suppressed at high temperatures due to self-sustaining coverage of the surface with segregated carbon layers from graphite substrate even under high heat flux plasma irradiation [2–5]. Nevertheless, data on hydrogen in high Z metal carbides are hardly available [6]. Therefore, it is quite important to investigate hydrogen behavior in refractory metal-carbon composite materials.

In a previous paper [7], we have reported the experimental results on retention and thermal re-emission of deuterium implanted into WC layers deposited on graphite plates. It has been shown that the steady state concentration of deuterium retained at room temperature is 1.7×10^{22} cm^{-3} which decreases to 1.4×10^{22} cm^{-3} due to the spontaneous re-emission within 5 h of terminating the implantation. It has been also found that the re-emission of retained D due to thermal annealing takes place in two stages: A large amount of D is re-emitted from the WC layers at lower temperatures and a small amount of the remainder is re-emitted from carbons in grain boundaries at high temperatures. The

* Corresponding author. Tel.: +81 52 789 4686; fax: +81 52 789 3791 5155; e-mail: k-morita@nucl.nagoya-u.ac.jp.

0022-3115/99/$ – see front matter
PII: S0022-3115(98)00518-2

isothermal re-emission profiles at different temperatures have been analyzed using the mass balance equations with a single trap in the WC layers.

In this paper, we report the experimental results on the thermal re-emission of protium implanted into the WC layers which are compared with those of deuterium. New results show that the re-emission of retained hydrogen isotopes due to thermal annealing takes place in three stages: large amounts of hydrogen are re-emitted from the two different traps in the WC layers at lower temperatures and a small amount is re-emitted from carbons in grain boundaries at higher temperatures which corresponds to the previous result [7].

2. Experimental

Isotropic graphite plates (IG-110U) of $0.5 \times 5 \times 35$ mm^3 in size were used as a substrate of the specimen. The surface of the graphite plate was polished with fine diamond paste on which a W-film of 400 nm in thickness was deposited by electron beam heating. The WC layers were prepared by direct current heating of the graphite substrate at 1400°C for 30 min. The specimen was characterized by means of the Rutherford backscattering spectroscopy (RBS) and the X-Ray diffraction (XRD) techniques. It was found that the average atomic composition of WC layers by RBS was $C/W = 0.96 \pm 0.04$ and the lattice constants for hexagonal lattice were also $a_0 = 2.93 \pm 0.01$ Å and $c_0 = 2.85 \pm 0.02$ Å. Since the WC layers were polycrystalline and the XRD analysis showed graphite peaks, a small fraction of carbon was expected to exist in grain boundaries.

In order to remove residual hydrogen, the specimen was heated at 1000°C for 10 min before protium implantations. The implantation into the WC layers was done with 5 keV H_2^+ ion beam up to saturation at room temperature and at a flux of 2.4×10^{13} cm^{-2} s^{-1}. The concentration of protium in the WC was measured by means of the elastic recoil detection technique [8], in which 1.7 MeV He^+ ion beam impinges on the WC at an angle of 85° to the surface normal and recoiled protons were also detected at a forward angle of 82° to the surface normal. An irradiation fluence of the probing He^+ ions for the ERD measurement was monitored by means of the RBS technique.

3. Experimental results

First of all, protium retention in the WC layers deposited on graphite irradiated with 5 keV H_2^+ ions was measured as a function of irradiation time. It was found, similarly to deuterium retention in the previous work [7], that the retained number of H increases rapidly at an early stage of irradiation and then saturates at a level which decreases by a factor of about 15% in several hours of terminating the irradiation due to spontaneous re-emission.

The retained number of H in the WC layers after isochronal annealings for 10 min is shown as a function of temperature in Fig. 1, where the retained number of D measured previously is shown for comparison and the vertical axis represents the retained number of H and D normalized by the initial saturation number, respectively. From Fig. 1, the re-emission of both H and D is seen to take place in three stages, which is for the first time recognised by comparison between the re-emission curves of H and D. The plot indicates that the first stage takes place at retained fractions of 1.0–0.6, the second stage at retained fractions of 0.6–0.2 and the last stage at retained fractions below 0.2, which is attributed to re-emission from the carbons in grain boundaries at higher temperatures.

Isothermal re-emission curves of H measured at different temperatures are shown as a function of annealing time in Fig. 2, where the vertical axis represents the retained number normalized by the initial saturation number. For comparison, isothermal re-emission curves of D measured in the previous work are shown in Fig. 3. It is clearly seen from Figs. 2 and 3 that the hydrogen concentrations decrease rapidly in the beginning of annealing and hereafter decrease very gradually with time and that there exists a clear isotope effect in the thermal re-emission. The analysis of the re-emission kinetics is described in Section 4.

4. Discussion

4.1. Analysis of thermal re-emission curves

The decay curves of the hydrogen concentration due to the isochronal annealing in Fig. 1 indicate that the

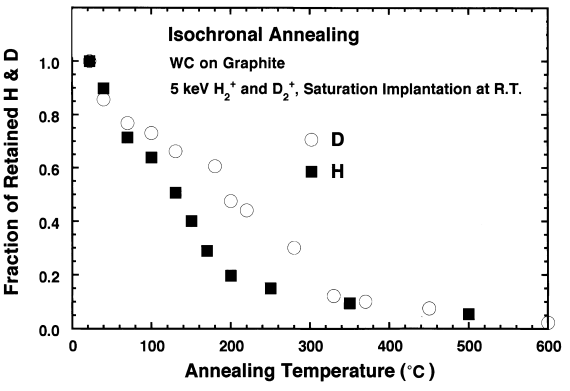

Fig. 1. Retention of protium (■) and deuterium (○) in a WC layer, implanted up to saturation at room temperature, after isochronal annealings for 10 min.

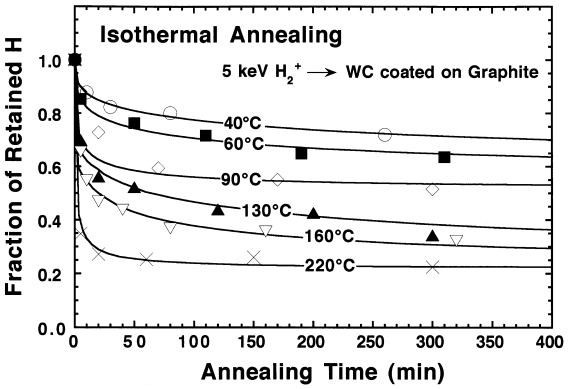

Fig. 2. Protium retention in a WC layer, implanted up to saturation at room temperature, during isothermal annealing at temperatures of 40°C, 60°C, 90°C, 140°C, 160°C and 220°C. The solid lines represent the best fitting curves calculated on the two-trap model.

re-emission takes place at three stages: the two stages at lower temperatures are ascribed to the re-emission of hydrogen atoms trapped in WC crystallites and the third stage at higher temperature is attributed to the re-emission of hydrogen atoms trapped in carbon segregated in the grain boundaries of the WC layers. Therefore, two different trapping sites should be taken into account for the analysis of the isothermal re-emission curves of hydrogen retained in WC crystallites.

The decay curves of the hydrogen concentration due to isothermal re-emission in Figs. 2 and 3 indicate that the concentration decreases rapidly in the beginning of the annealing and hereafter gradually with time. The initial rapid decay is ascribed to no retrapping of thermally detrapped hydrogen due to no existence of available trapping sites because of saturation implantation. The late slow decay is attributed to strong retrapping of thermally detrapped hydrogen into vacant trapping sites produced by the initial decay. Almost no decays of both protium at 220°C in Fig. 2 and deuterium at 350°C in Fig. 3 for prolonged annealing indicate that the remaining protium and deuterium are trapped in the deeper trap. This fact corresponds well to the isochronal re-emission curves in Fig. 1. Therefore, the decay of the hydrogen concentration in WC crystallites should be analyzed by solving the mass balance equations governing the time evolution of the concentrations of hydrogen migrating freely and trapped in two kinds of trapping sites which take into account the following elementary processes: thermal detrapping, retrapping and local molecular recombination between free species leading to the re-emission. The mass balance equations are described in the following forms:

$$\frac{dn(t)}{dt} = \Sigma_{d_1} n_{T_1}(t) + \Sigma_{d_2} n_{T_2}(t) - \Sigma_T n(t)[C_o - n_{T_1}(t) - n_{T_2}(t)] - 2K_1 n^2(t), \quad (1)$$

$$\frac{dn_{T_1}(t)}{dt} = -\Sigma_{d_1} n_{T_1}(t) + \Sigma_T n(t)[C_1 - n_{T_1}(t)], \quad (2)$$

$$\frac{dn_{T_2}(t)}{dt} = -\Sigma_{d_2} n_{T_2}(t) + \Sigma_T n(t)[C_2 - n_{T_2}(t)], \quad (3)$$

where n(t), $n_{T_1}(t)$ and $n_{T_2}(t)$ are the average concentrations of hydrogen migrating freely and trapped in the trapping sites T_1 and T_2, respectively. Σ_{d_1} and Σ_{d_2} are the thermal detrapping rate constants for the trapping sites T_1 and T_2, respectively, Σ_T is the trapping rate constant, K_1 is the local molecular recombination rate constant, C_0 ($= C_1 + C_2$) is the total trap density, here C_1 and C_2 are the densities of the trapping sites T_1 and T_2. The assumption of local molecular recombination is based on the fact that the decay of retained hydrogen takes place uniformly over the whole depth of the WC layers. When the concentration of free hydrogen is assumed to attain to a quasi-equilibrium, namely, $dn(t)/dt = 0$, the following equation is derived from Eqs. (1)–(3):

$$\frac{d[n_{T_1}(t) + n_{T_2}(t)]}{dt} = -\frac{2K_1[\Sigma_{d_1} n_{T_1}(t) + \Sigma_{d_2} n_{T_2}(t)]^2}{\Sigma_T^2[C_o - n_{T_1}(t) - n_{T_2}(t)]^2}. \quad (4)$$

(a) Stage 1 (low temperature): When the thermal detrapping takes place mainly from the shallower trapping sites ($\Sigma_{d_1} \gg \Sigma_{d_2}$) at low temperature, the concentration of hydrogen trapped in the deeper trapping site is hardly reduced, thus $n_{T_2}(t)$ being assumed to be constant. In such a case the decay kinetics of hydrogen at the low temperature is expressed by the following equation as a solution of Eq. (4).

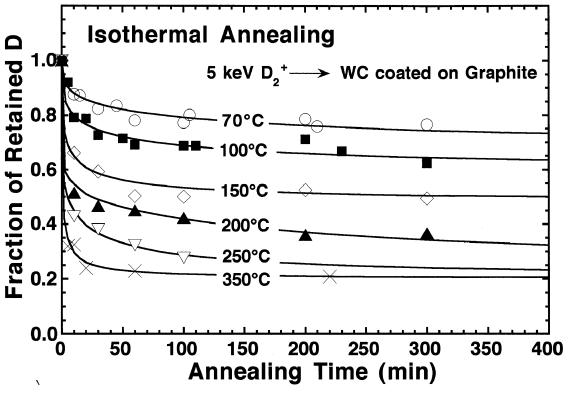

Fig. 3. Deuterium retention in a WC layer, implanted up to saturation at room temperature, during isothermal annealing at temperatures of 70°C, 100°C, 150°C, 200°C, 250°C and 350°C. The solid lines represent the best fitting curves calculated based on the two-trap model.

$$[1-(1-a)N_{T_2}(t)]^2 \left[\frac{1}{1-(1-a)N^0_{T_2}}-\frac{1}{N_T(t)-(1-a)N_{T_2}(t)}\right] - 2[1-(1-a)N_{T_2}(t)]\ \ln\left[\frac{N_T(t)-(1-a)\,N_{T_2}(t)}{1-(1-a)\,N^0_{T_2}}\right] + \left\{N_T(t)-1+(1-a)[N_{T_2}(t)-N^0_{T_2}]\right\} = -2\frac{K_1}{C_0}\left(\frac{\Sigma_{d_1}}{\Sigma_T}\right)^2 t, \quad (5)$$

where $a=\Sigma_{d_1}/\Sigma_{d_2}$ and $N_T(t)=N_{T_1}(t)+N_{T_2}(t)=[n_{T_1}(t)+n_{T_2}(t)]\ /\ n_0$. It is seen from Eq. (5) that the value of $(K_1/C_0)(\Sigma_d/\Sigma_T)^2$ is determined by the best fit of Eq. (5) to the experimental isothermal re-emission curve for the fitting parameter a when $N_{T_2}(t)$ is given. The value of $N_{T_2}(t)$ can be extrapolated from the experimental data at the high temperatures described below.

(b) Stage 2 (high temperature): When the thermal detrapping takes place from the deeper trapping sites, only the retrapping into the deeper trapping sites plays an important role in the re-emission curve. Except at the beginning of the annealing, it may be assumed that $N_{T_1}(t)=0$. In this case, the decay kinetics of hydrogen at the high temperature is also expressed by the following equation as a solution of Eq. (4).

$$\frac{C_0}{n_0}\left[\frac{1}{N^0_{T_2}}-\frac{1}{N_{T_2}}(t)\right]-2\ \ln\left[\frac{N_{T_2}(t)}{N^0_{T_2}}\right] + \frac{n_0}{C_0}[N_{T_2}(t)-N^0_{T_2}] = -2\frac{K_1}{C_0}\left(\frac{\Sigma d_2}{\Sigma_T}\right)^2 t, \quad (6)$$

where $n_0=n^0_{T_1}+n^0_{T_2}$. It is seen from Eq. (6) that the value of $(K_1/C_0)(\Sigma_{d_2}/\Sigma_T)^2$ is determined by the best fit of Eq. (6) to the experimental re-emission curve with fitting parameter $N^0_{T_2}$.

4.2. Rate constants of elementary processes

In order to obtain the rate constants Σ_{d_1} and Σ_{d_2}, and $(K_1/C_0)(\Sigma_{d_1}/\Sigma_T)^2$ and $(K_1/C_0)(\Sigma_{d_2}/\Sigma_T)^2$, Eqs. (5) and (6) were fitted to the experimental data in Figs. 2 and 3. First of all, the thermal detrapping rate constant Σ_{d_1} for the shallower trapping site was determined from the initial decay of the curves at low temperatures (40°C, 60°C, 90°C and 130°C in Fig. 2 and 70°C, 100°C, 150°C in Fig. 3), which are produced by the thermal detrapping-limited process because of no available trapping sites. The values obtained are shown as function of 1000/T (K) in Fig. 4.

Secondly, the values of $(K_1/C_0)(\Sigma_{d_2}/\Sigma_T)^2$ were determined by assuming as fitting parameter N^0_c, the fraction of hydrogen atoms which are retained in carbon segregated in grain boundaries of WC crystallites. The

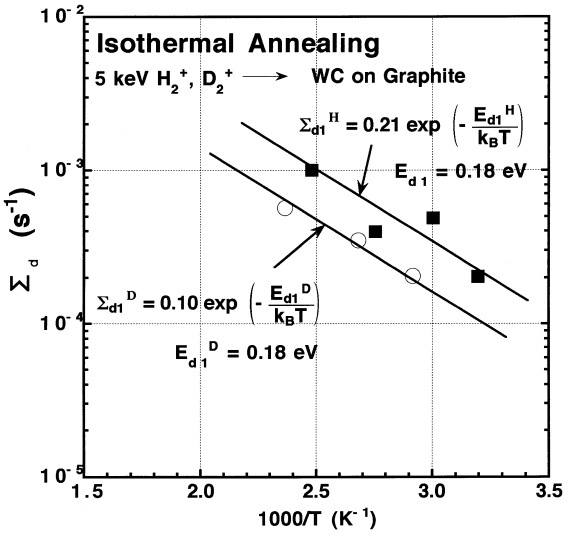

Fig. 4. Arrhenius plot of the experimental values of $\Sigma^H_{d_1}$ (□) and $\Sigma^D_{d_1}$ (○) vs. 1000/T.

best fit was achieved so that the values on the left-hand side of Eq. (6) calculated by substitution into $N_{T_2}(t)$ of the experimental data at high temperatures (130°C, 160°C and 220°C in Fig. 2 and 200°C, 250°C and 350°C in Fig. 3) subtracted by N^0_c (roughly 0.2 from Fig. 1) and with the fitting parameter $N^0_{T_2}$ were proportional to annealing time. For fitting, it was assumed that $n_0/c_0=1$, since the initial hydrogen concentration was at the saturation level. It is seen from Figs. 2 and 3 that the best fitting curves reproduce the experimental re-emission data well. It follows from the fitting that 20% of the total retained deuterium and 22% of the total retained protium, namely about 3×10^{21} cm^{-3}, were trapped in carbon segregated in the grain boundaries. This fact indicates that the effective volume of carbon in the grain boundaries is several % of the WC layers, which might include carbon-interstitial clusters produced by the hydrogen ion implantation. It was also found that N^0_{T2} was about 0.4–0.5. This fact indicates that the fraction of the deeper trapping site is one half.

Finally, the values of $(K_1/C_0)(\Sigma_{d_1}/\Sigma_T)^2$ were determined by fitting Eq. (5) to the experimental data at low temperature with use of $N_{T_2}(t)$ calculated from Eq. (6) and the values of $(K_1/C_0)(\Sigma_{d_2}/\Sigma_T)^2$ obtained above for the parameter a. Under the best fitting condition, it was found that $a\sim0$. This fact indicates that Σ_{d_2} cannot be determined in this procedure. The values of $(K_1/C_0)\times(\Sigma_{d_1}/\Sigma_T)^2$ are shown as a function of 1000/T (K) with those of $(K_1/C_0)(\Sigma_{d_2}/\Sigma_T)^2$ in Figs. 5 and 6, where for comparison the values of $(K_1/C_0)(\Sigma_d/\Sigma_T)^2$, based on the single-trap model, are shown by dotted lines.

It is seen from Figs. 5 and 6 that the values of $(K_1/C_0)(\Sigma_d/\Sigma_T)^2$ obtained on the single-trap model approach the values of $(K_1/C_0)(\Sigma_{d_1}/\Sigma_T)^2$ for the shal-

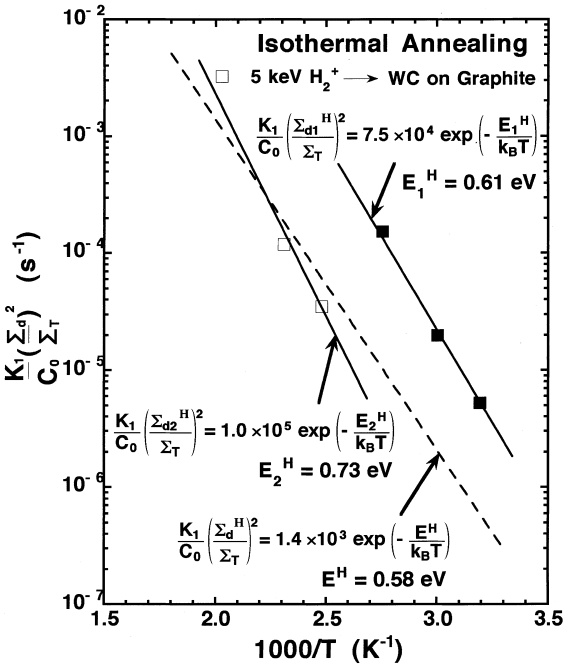

Fig. 5. Arrhenius plot of the effective recombination rate constants for deuterium $(K_1/C_o)(\Sigma^D_{d_1}\Sigma/T)^2$ for shallower trapping site and $(K_1/C_o)(\Sigma^D_{d_2}/\Sigma_T)^2$ for deeper trapping site. The dashed line is the effective recombination rate constant calculated by the single-trap model.

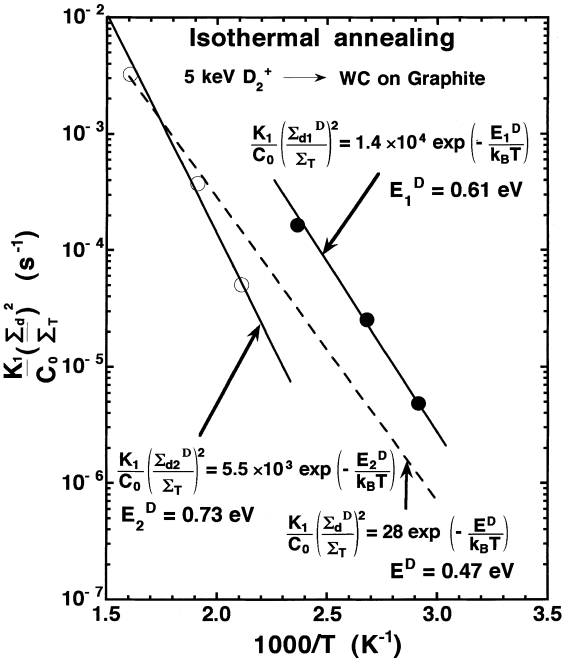

Fig. 6. Arrhenius plot of the effective recombination rate constants for deuterium $(K_1/C_o)(\Sigma^D_{d_1}\Sigma/T)^2$ for shallower trapping site and $(K_1/C_o)(\Sigma^D_{d_2}/\Sigma_T)^2$ for deeper trapping site. The dashed line is the effective recombination rate constant calculated by the single-trap model.

lower trap at low temperatures and are close to the values of $(K_1/C_0)(\Sigma_{d_2}/\Sigma_T)^2$ at high temperatures. The fit of the theoretical to the experimental re-emission curves achieved by the two-trap model were found to be much better than those on the single-trap model. Therefore, from these facts, the decay analysis of the two-trap model is considered to be reasonable. It is also seen from Figs. 5 and 6 that the value of the activation energy of the effective recombination rate constants $(K_1/C_0)(\Sigma^H_{d_1}/\Sigma_T)^2$ for protium in the shallower trapping site is the same as that, $(K_1/C_0)(\Sigma^D_{d_1}/\Sigma_T)^2$, for deuterium and the ratio of their absolute values is 5.4. On the other hand, it is seen from Fig. 4 that the value of the activation energy $E^H_{d_1}$ of the thermal detrapping rate constants for protium is the same as that, $E^D_{d_1}$ for deuterium and the ratio of the absolute values is about 2. Therefore, the isotope difference in the effective recombination rate constants is mainly ascribed to the isotope difference in the thermal detrapping rate constants.

It is also seen from Fig. 4 that the activation energy of the thermal detrapping rate constants $\Sigma^H_{d_1}$ and $\Sigma^D_{d_1}$ for the shallower trapping site is 0.18 eV. Although the thermal detrapping rate constants $\Sigma^H_{d_2}$ and $\Sigma^D_{d_2}$ for deeper trapping site could not be determined directly by the fitting, the activation energy can be estimated to be 0.24 eV from Figs. 5 and 6 using the $E^H_{d_1} = E^D_{d_1} = 0.18$ eV. These activation energies are considerably small compared with those (0.60 eV) in graphite [8]. Therefore, in the fitting, it is very reasonable to assume that the hydrogen atoms are not re-emitted from carbon segregated in the grain boundaries of the WC layer.

The trapping sites with such small trapping energies obtained above are not considered to be vacancies nor carbon interstitial clusters produced by hydrogen ion implantation, but to be intrinsic interstitial sites in the WC lattice. There exist two different hexahedral interstitial sites in a WC unit cell, which are formed by two different atomic clusters: one type cluster is composed of three carbon atoms and two tungsten atoms and the other type of three tungsten atoms and two carbon atoms. Since the two clusters are adjoined with each other, there must exist six vacant interstitial sites around one filling interstitial site in order for hydrogen to be stably trapped in an interstitial site. In the fitting, each fraction of shallower and deeper trapping sites was found to be a half, as described above. The fraction of retained hydrogen to WC molecule was also found to be 0.24 in the previous work [7]. This value indicates that about 8.4 vacant interstitial sites exist around one hydrogen filling interstitial site. Thus the observations seem to indicate that the above consideration is effec-

tive. It is not clear which type cluster is shallower or deeper energetically.

References

[1] A. Santaniello, J. Appelt, J. Bohdansky, J. Roth, J. Nucl. Mater. 162–164 (1989) 951.
[2] S. Sukenobu, Y. Gomay, H. Ohno, K. Morita, J. Nucl. Mater. 148 (1987) 66.
[3] K. Morita, K. Mori, Y. Muto, J. Nucl. Mater. 196–198 (1992) 564.
[4] S. Takamura, K. Yamamoto, K. Morita, Jpn. J. Appl. Phys. 37 (1998) 266.
[5] S. Takamura, K. Hayashi, N. Ohno, K. Morita, J. Nucl. Mater. 258–263 (1998) 961.
[6] W. Wang, V.Kh. Alimov, B.M.U. Scherzer, J. Roth, J. Nucl. Mater. 241–243 (1997) 1087.
[7] T. Horikawa, B. Tsuchiya, K. Morita, J. Nucl. Mater. 258–263 (1998) 1087.
[8] K. Morita, Y. Muto, J. Nucl. Mater. 196–198 (1992) 963.